Delamination of organically modified montmorillonite for reducing the filler networking with carbon black in poly(1,4-*cis*-isoprene) based nanocomposites

Maurizio Galimberti [a,*], Michele Coombs [a,1], Stefano Pandini [b], Theonis Riccò [b], Valeria Cipolletti [a], Lucia Conzatti [c], Gaetano Guerra [d]

[a] *Politecnico di Milano, Via Mancinelli 7, 20131 Milano, Italy*
[b] *Università degli Studi di Brescia, Via Branze 38, 25123 Brescia, Italy*
[c] *Consiglio Nazionale delle Ricerche, Istituto per lo Studio delle Macromolecole, Via De Marini 6, 16149 Genova, Italy*
[d] *Università degli Studi di Salerno, Via Giovanni Paolo II 132, 84084 Fisciano (SA), Italy*

Received 24 February 2014
Received in revised form 5 November
2014 Accepted 13 November 2014
Available online 6 December 2014

1. Introduction

Clay polymer nanocomposites (CPN) (Alexandre ad Dubois, 2000; Bergaya, 2008; Chen et al., 2008; Galimberti, 2011; LeBaron et al., 1999; Ray and Okamoto, 2003) are gaining increasing importance as substantial improvement of polymer properties, such as mechanical re-inforcement, impermeability and thermal stability (Galimberti et al., 2013a; Paul and Robeson, 2008), is achieved when the clays are evenly dispersed in the polymer matrix. CPN have been already largely used in the field of soft materials, as for example elastomeric composites, even for demanding dynamic-mechanical applications such as the one for tyre compounds (Galimberti et al., 2013a). In this field, clay or clay mineral does not completely replace traditional fillers such as carbon black (CB) and silica but is used in partial substitution, giving rise to CPN based on a hybrid filler system, in particular with CB.

In the scientific literature various authors have focused their attention on clay/CB hybrid systems in different elastomeric matrices, such as poly(1,4-*cis*-isoprene), both synthetic (PI) (Galimberti et al., 2012, 2013b) and naturally occurring (NR), used as the only polymer (Das et al., 2010; Galimberti et al., 2009) or in blend with poly(styrene-*co*-butadiene) (Cataldo, 2007), epoxidized NR (Chattopadhyay et al., 2011), chlorinated NR (Sridhar et al., 2009), poly(styrene-*co*-butadiene)(Gopi et al., 2011; Maiti et al., 2005; Praveen et al., 2009), brominated poly(isobutylene-*co*-paramethylstyrene) (Maiti et al., 2005), and poly(ethylene-*co*-propylene) (Malas and Das, 2012). Synergistic effect on the mechanical reinforcement, between clay mineral and CB, was reported (Das et al., 2010; Galimberti et al., 2012, 2013b; Praveen et al., 2009) and very low amounts of clay mineral were shown to have a profound effect on the dynamic-mechanical properties of the

* Corresponding author at: Politecnico di Milano, Via Mancinelli 7, 20131 Milano, Italy. Tel.: +39-02-2399-4746; fax: +39-02-2399-3180.
E-mail address: maurizio.galimberti@polimi.it (M. Galimberti).
[1] Present address: Pirelli Tyre, Viale Sarca 222, 2016 Milano, Italy.

CPN (Galimberti et al., 2012). To explain these findings, the formation of hybrid filler networks was proposed (Galimberti et al., 2012, 2013b). The intimate interaction between CB and a nanofiller could be expected on the basis of zeta potential (ZP) measurements (Bhattacharya and Bhowmick, 2010): it was shown that ZP of nanofillers are negative in the pH range of elastomeric composites, whereas those of CB are positive (Gates, 2004; Kvandea et al., 2008; Lin et al., 2006; Sabah et al., 2007; Xu et al., 2007). It was reported that ZP can be also applied to polymer melts (Brochard-Wyart and de Gennes, 2000; Flores et al., 2007) and the affinity of clay mineral for CB was particularly shown (Feller et al., 2004; Konishi and Cakmak, 2005).

Moreover, a recent paper (Galimberti et al., 2013c) hypothesized that a cation–pi interaction between the compensating cation of clay mineral and CB lies at the origin of the synergism: montmorillonite (Mt) was organically modified (OMt) with organophilic ammonium cations, in order to promote the compatibilization of the polar filler with the apolar matrices.

Results available in the prior art propose thus a reasonable structure–property correlation for CPN based on this hybrid filler system. However, it is widely acknowledged that the effects of OMt in CPN depend on their organization in the polymer matrix. To understand and predict the behavior of CPN, aspects such as clay mineral distribution and dispersion and especially the intimate clay mineral organization, namely the extent of clay mineral delamination in the polymer matrix, have to be assessed.

The objective of this work was to achieve a deeper knowledge of the structure–property correlation of polymer materials based on the clay mineral/CB hybrid filler system. In particular, the effect of clay mineral delamination on the dynamic-mechanical properties of the nanocomposites was investigated. This paper adopts the definition of delaminated and exfoliated clay minerals given in recent papers (Bergaya and Lagaly, 2011; Bergaya et al., 2011): an appreciable interac-tion between two successive layers remains in delaminated clay min-erals, with some maintained crystallographic orientation, whereas no interaction, between isolated layers or stackings of few layers, is left in exfoliated clay minerals (Bergaya et al., 2012).

In this work, CPN were prepared by melt blending PI and OMt hav-ing dimethylditallow ammonium (2HT) as the compensating cation. Two types of OMt were used: intercalated OMt (I-OMt), with the am-monium cation intercalated in the interlayer space, and an extensively delaminated OMt (D-OMt), prepared by ball milling I-OMt. The crystal-line structure of OMt was studied by means of X-ray diffraction (XRD) analysis and the structure of CPN was investigated through XRD and transmission electron microscopy (TEM). Dynamic-mechanical proper-ties were assessed, through shear measurements, for uncrosslinked masterbatches and for nanocomposites crosslinked with sulfur based systems, performing strain sweep tests, determining the time needed to recover the initial modulus after a large strain perturbation, deriving mastercurves for the dependence of the storage modulus on the frequency.

2. Experimental

2.1. Materials

2.1.1. Fillers

OMt was Dellite® 67G from Laviosa Chimica Mineraria S.p.A., with dimethylditallow ammonium (2HT) as the compensating cation and 55 and 45 as mass% of Mt and of the ammonium moiety, respectively. This amount of ammonium cation corresponds to 140 mmol/100 g of Mt. This value appears to be higher than CEC of pristine Mt provided by the same company. Ball milling of OMt was performed with a plane-tary ball mill S100 from Retsch, with the 0.3 l grinding jar moving in horizontal plane. 6 ceramic balls with a diameter of 20 mm and 10 g of OMt were put into the jar that was allowed to rotate at 100 rpm, at room temperature, for 24, 72, 168 or 240 h.

Carbon black N326 (CB) was from Cabot, with the following charac-terization data: 30 nm as mean diameter of spherical primary particles, surface area from nitrogen adsorption of 77 m^2/g and DBP adsorption number of 85 ml/100 g.

2.1.2. Ingredients for nanocomposites' preparation

Synthetic poly(1,4-*cis*-isoprene) (PI) (Nizhnekamskneftechim Export) had trade name SKI3 and 70 Mooney units (MU) as Mooney viscosity ($M_L(1 + 4)100$ °C). 3-Octanoylthio-1-propyltriethoxysilane (silane NXT) (Momentive), ZnO (Zincol Ossidi), stearic acid (Sogis), *N*-(1,3-dimethylbutyl)-*N′*-phenyl-*p*-phenylenediamine (6PPD) (Cromp-ton), sulfur (Solfotecnica), *N*-cyclohexylbenzothiazol-2-sulfenamide (CBS) (Flexsys), *N*-cyclohexylthiophthalimide (premature vulcaniza-tion inhibitor, PVI) (Flexsys) and phthalic anhydride (Aldrich) were used as received.

2.2. Preparation of PI/CB and PI/CB/OMt composites

Formulations of composites are reported in Table 1. Composites were prepared in a Banbury® type internal mixer hav-ing a volume of 1050 cm^3, as follows. 738 g of PI were introduced into the mixer at 60 °C and masticated for 30 s with rotors rotating at 75 rpm. CB was then added: 442.8 g (60 phr) to prepare the CB based composite and 369 g (50 phr) to prepare CB–I-OMt and CB–D-OMt nanocomposites. Mixing was then carried out for 150 s. The resulting masterbatches were discharged at about 110 °C and were stored at room temperature for about 16 h. They were then introduced into the same mixer at 80 °C and masticated at 30 rpm for 60 s. In the case of nanocomposites CB–I-OMt and CB–D-OMt, 61.3 g (8.3 phr) of I-OMt and D-OMt were then added. This amount corresponds to the same vol-ume fraction of 10 phr of CB. Mixing was then carried out, for the three masterbatches, for 240 s, discharging them at about 90 °C. Composites were then fed again to the mixer together with ZnO, stearic acid and 6PPD and mixing was performed at 50 °C for 120 s. The other ingredi-ents (S, CBS, phthalic anhydride, PVI) were finally added, performing a further mixing at 50 °C for 180 s. The compounds were finally homoge-nized by passing them 5 times on a two roll mill, with the front roll rotating at 30 rpm and the back roll at 38 rpm. Curing was carried out at 170 °C for 20 min under a pressure of 150 bar.

2.3. Characterization of Mt, OMt and CPN

2.3.1. X-ray diffraction analysis

Wide-angle X-ray diffraction (WAXD) patterns with nickel filtered Cu-Kα radiation were obtained in reflection, with an automatic Bruker D8 Advance diffractometer. Patterns were recorded in 2°–80° as the 2θ range, 2θ being the diffraction peak angle. For the clay mineral, the intensities of the WAXD patterns, after subtraction of the tail of the

Table 1
Formulations of PI based composites containing CB and OMt.[a,b,c]

Ingredient	Composites		
	CB	CB–I-OMt	CB–D-OMt
PI	100	100	100
CB	60	50	50
I-OMt	0	8.3	0
D-OMt	0	0	8.3
Silane[d]	0.8	0.8	0.8

[a] I-OMt: intercalated OMt and D-OMt: delaminated O-Mt.
[b] Amount of ingredients are indicated in phr (part per hundred polymer).
[c] Further ingredients: ZnO (4 phr); stearic acid (2 phr); 6PPD (2 phr); sulfur (2 phr); CBS (1.8 phr); phthalic anhydride (1 phr); and PVI (0.3 phr).
[d] 3-Octanoylthio-1-propyltriethoxysilane.

primary beam, were corrected for polarization and Lorentz factors, by using the following equation:

$$I_{cor.} = I_{exp.}/\left\{\left[\left(1 + \cos^2 2\theta\right)/2\right] * \left[\left(\sin^2\theta * \cos\theta\right)/2\right]\right\} \quad (1)$$

where: $I_{cor.}$ is the corrected diffraction peak intensity and $I_{exp.}$ is the diffraction peak experimental intensity. For a better comparison with literature data, these intensity corrections were not applied to WAXD patterns of the CPN.

Reported XRD patterns were normalized with respect to the 060 reflection. The $D_{hk\ell}$ correlation length of crystals was determined applying the Scherrer equation

$$D_{hk\ell} = K\lambda/(\beta_{hk\ell}\cos\theta_{hk\ell}) \quad (2)$$

where: K is the Scherrer constant, λ is the wavelength of the irradiating beam (1.5419 Å, Cu-Kα), $\beta_{hk\ell}$ is the width at half height, and $\theta_{hk\ell}$ is the diffraction angle. The instrumental broadening, b, was also determined by obtaining a WAXD pattern of a standard silicon powder 325 mesh (99%), under the same experimental conditions. For each observed reflection with $\beta_{hk\ell} < 1°$, the width at half height, $\beta_{hk\ell} = (\beta_{hk\ell} - b)$, was corrected by subtracting the unavoidable instrumental broadening of the closest silicon reflection from the experimental width at half height, $\beta_{hk\ell}$.

2.3.2. Transmission electron microscopy (TEM)

TEM analysis of composites was performed with a Zeiss EM 900 microscope applying an accelerating voltage of 80 kV. Ultrathin sections (about 50 nm thick) were obtained by using a Leica EM FCS cryoultramicrotome equipped with a diamond knife (sample temperature: −130 °C).

2.3.3. Differential scanning calorimetry (DSC)

DSC analyses were performed with a Mettler 823e instrument. OMt or CPN sample (7–12 mg) was placed in a sealed aluminum pan and heating–cooling–heating runs from −20 to 150 °C were performed at 10 °C/min.

2.3.4. Shear dynamic-mechanical measurements

DMA Q800 TA Instruments was used to measure dynamic-mechanical properties of the composites. Tests were performed using the device shown in Fig. 1, in which the composite specimen of about 2.0 × 8.0 × 4.0 mm was sandwiched between two aluminum plates.

Good grip between the aluminum plates and the composite specimen was assured by means of acrylic glue, in order to avoid any pressure of the aluminum plate on the specimen during measurements and undesired stresses that may contribute to the evaluation of the Payne effect. The experimental procedures are described as follows, as a function of the dynamic test.

2.3.5. Strain sweep tests

Samples were kept in the instrument, at the smallest strain amplitude (1 μm = 0.1%), for 330 min, to allow the sample to achieve fully equilibrated conditions of mechanical properties. A Strain sweep experiment was then performed, with 0.1–30% as the strain amplitude range and a frequency of 1 Hz. Three samples were examined for each composite, in order to calculate variation coefficients.

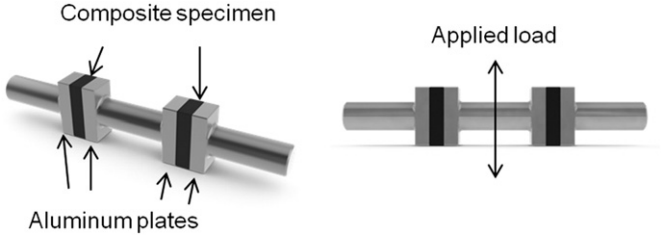

Fig. 1. Device used to measure shear dynamic-mechanical properties.

Additional strain sweep tests, reported below in the text in Fig. 8, were performed with a Monsanto R.P.A. 2000 rheometer in the torsion mode. For each sample, a first strain sweep (0.1–30% shear strain ampli-tude) was performed at 50 °C and 1 Hz, then the sample was kept in the instrument at the minimum strain amplitude (γ_{min} = 0.1%) for 10 min, to achieve fully equilibrated conditions. Finally, dynamic tests were performed at 50 °C at increasing strain amplitude (0.1–30% shear strain amplitude) with a frequency of 1 Hz.

2.3.6. Recovery tests

The low strain amplitude (γ) dynamic modulus recovery, subsequent to the application of a high amplitude dynamic strain, was inves-tigated by adopting the following procedure. The storage modulus at low strain amplitude (γ = 0.003) was first determined, at 5 Hz frequen-cy, and was taken as the reference value of low amplitude storage mod-ulus. A high amplitude dynamic strain (γ = 0.1) was then applied, at the same frequency. Finally the specimen was subjected again to a low amplitude dynamic strain, with a strain amplitude of 0.003, and the evo-lution of the modulus was measured as a function of time for 2 h. A delay of 20 s occurred between the application of the high amplitude pertur-bation and the first dynamic test at low amplitude.

2.3.7. Determination of the master curve

Multifrequency tests were performed on uncrosslinked master-batches containing only PI, the silane and either D-OMt or I-OMt. Shear strain with amplitude of 0.1% was imposed to specimens, cyclical-ly sweeping two decades of frequency (0.3, 1, 3, 10, 30 Hz) and contin-uously increasing the temperature from −50 to 100 °C. This allowed obtaining quasi-isothermal representations of the frequency depen-dence of the storage modulus G′. Collected data were elaborated by TA Instruments Rheology Advantage Data Analysis software and, by a tentative application of the time-temperature superposition (TTS) principle, it was possible to provide a master curve representations of the G′ dependence on frequency. The temperature of −45 °C was cho-sen as the reference temperature for the translation of experimental points along the frequency axis.

3. Results and discussion

3.1. Intercalated and delaminated OMt

I-OMt was commercially available (Dellite® 67G) and was Mt with 2HT as the intercalated ammonium cation. D-OMt was prepared via ball milling of I-OMt, as described in the experimental part. In the literature there are reports of the ball milling of pristine clays such as bentonite (Christidis et al., 2004), Na–Mt (Ramadan et al., 2010) and Ca–Mt (Dellisanti and Valdre, 2005; Hrachova et al., 2007). Effects on crystallite size and structure were not reported for bentonite but were clearly observed in Ca–Mt (Dellisanti and Valdre, 2005) with also a complete breakdown of the mineral layers (Hrachova et al., 2007). The (001) reflection disappeared from the XRD pattern of Na–Mt, after some hours of ball milling. Milling was also reported for OMt con-taining different compensating cations: octadecyltrimethylammonium (Hrachova et al., 2007) and di(hydroxyethyl)tallow ammonium (Ramadan et al., 2010). In both research works, delamination of OMt was documented.

Fig. 2 shows XRD patterns in the 2θ range 2–80° of I-OMt and D-OMt samples, also with a zoom on the (00ℓ) reflections, whose intensities have been corrected for polarization and Lorentz factors.

I-OMt shows a high degree of order in the direction orthogonal to the structural layers, as indicated by the presence of (001), (002), (003) and (004) reflections, at 2.50°, 4.66°, 7.23° and 9.80° as 2θ values, respectively, that allow the calculation of a d-value d_{001} = 3.53 nm. The

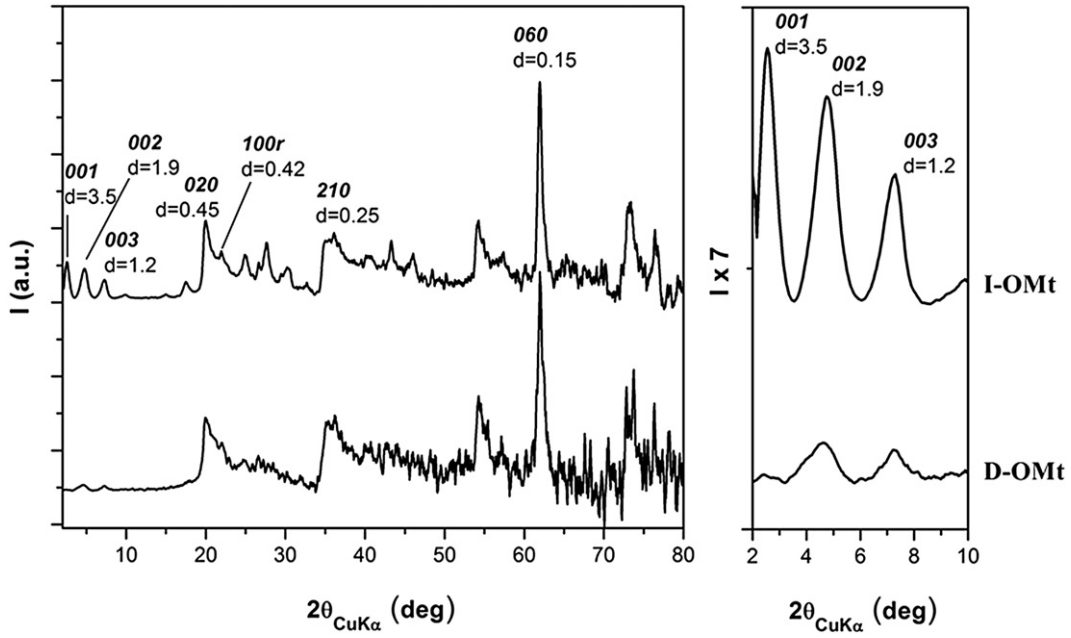

Fig. 2. XRD patterns in the 2θ range 2–80° of OMt samples, before milling (I-OMt) and after milling (D-OMt). Zoom on (00ℓ) reflections is in the right part of the figure.

clay mineral interlayer distance depends on the arrangement of the intercalated alkylammoniums. It is known (Lagaly et al., 2013) that dialkylammoniums give rise to paraffin-type arrangements with differ-ent tilting angles. By considering the obtained d_{001} value, the thickness of the clay mineral layer (≈1 nm) and the length of 2HT (≈2.5 nm)(Osman et al., 2002), the tilting angle of the hydrocarbon chains in the paraffin-type arrangement is estimated at 60°. By applying the Scherrer equation to the (001) reflection, the correlation length of crystals orthogonal to the layers was calculated to be close to 21 nm. A well de-fined narrow reflection is present at $2\theta = 21.7°$, with a distance be-tween crystallographic planes, equal to 0.42 nm, corresponding to the distance between *n*-alkanes in their rotator order (Chazhengina et al., 2003; Fu et al., 2011; Ungar and Masic, 1985). Such rotator order for long hydrocarbon chain has been recently reported for Mt (Cipolletti et al., 2014; Galimberti et al., 2013d) and for graphite oxide (Mauro et al., 2013) intercalate compounds containing 2HT chains in the inter-layer space. It is thus worth observing that the high density on the clay mineral surface of the ammonium compensating cations leads to the high order in the packing of the paraffinic chains. XRD pattern of I-OMt shows also well defined reflections due to the typical (020),(210) and (060) in-plane Mt periodicities (Galimberti et al., 2007; Powder diffraction database 70-2151).

The intensity of (00ℓ) reflections is remarkably reduced in the XRD pattern of D-OMt. This indicates extensive delamination, whose quantitative evaluation was attempted by defining a relative index of delamination (DI), given by the following expression:

$$DI = \left[1 - \left(R_{(\text{D-OMt})} / R_{(\text{I-OMt})}\right)\right] \cdot 100 \quad (3)$$

where $R = A_{(001)} / A_{(060)}$ and $A_{(hk\ell)}$ was the area of the peak related to ($hk\ell$) reflection.

By determining R in I-OMt ($R_{(\text{I-OMt})}$) and in D-OMt ($R_{(\text{D-OMt})}$), the delamination index was found to be close to 97%.

Reflections due to in-plane periodicities are not substantially affected by the milling process. In fact, the ratio between the areas of (020) and (060) reflections for D-OMt and I-OMt is close to 1 and to 0.9, respectively. It is worth noting that the reflection corresponding to the rotator order of the long hydrocarbon chains is evident also in the OMt sample milled for 240 h. These findings reveal that D-OMt prepared through ball milling is largely exfoliated and has the same crystalline order in the structural layer and also analogous order in the packing of the ammonium paraffinic tails.

DSC analysis was performed on I-OMt and on D-OMt. A clear endothermic phenomenon was detected for I-OMt in the first DSC scan, with a peak at about 48 °C, in line with what recently reported (Cipolletti et al., 2014), whereas phenomena were not revealed by thermographs of D-OMt. It is known that OMt with intercalated alkylammoniums experience endothermic transitions, commented as two-dimensional melting (Osman et al., 2002), occurring through the increase of the gauche population of paraffinic chains. Such endothermic transitions were observed also in anionic clays intercalated with long chain fatty acids (Itoh et al., 2003) as well as in graphite oxide intercalation compounds with alkylammoniums (Mauro et al., 2013). Thanks to the attribution of the reflection at $2\theta = 21.7°$ to the rotator order of polymethylene chains (Cipolletti et al., 2014), it is possible to comment that the endothermic transition experienced by I-OMt is due to the loss of order in the packing of the ammonium hydrocarbon tails.

3.2. Structure of CPN

CPN were prepared with PI as the polymer matrix, CB as the main filler and either I-OMt or D-OMt. 3-Octanoylthio-1-propyltriethoxysilane was used to favor OMt dispersion in the poly-mer matrix. Formulations, reported in Table 1, were conceived in order to investigate the effect on the CPN properties of the partial substitution of CB with OMt characterized by different delamination degree.

Structure of CPN was studied with the help of XRD and TEM analyses. The XRD patterns of masterbatches containing CB, silane and either I-OMt or D-OMt are reported in Fig. 3aand brespectively(00ℓ)reflections of the OMt are clearly visible in the pattern of the masterbatch with I-OMt whereas they are hardly detectable in that of the masterbatch with D-OMt. It is worth noting that (00ℓ)reflections are at the same 2θ values in the XRD patterns of pristine I-OMt and of the masterbatch with I-OMt. This indicates that polymer chains are not intercalated between the clay mineral layers of I-OMt. XRD analysis was also performed on the crosslinked nanocomposites, containing all the other ingredients indicated in Table 1. As far as the (00ℓ)reflections of the OMt are concerned, the same patterns were observed. The results of XRD investigation confirm that nanocomposites with either I-OMt

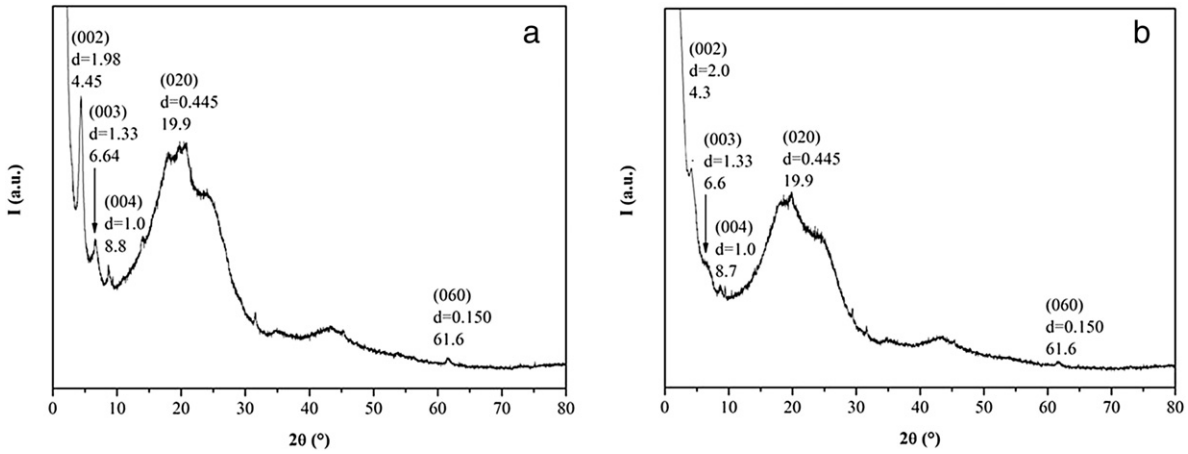

Fig. 3. XRD patterns of PI-based masterbatches, containing CB, silane and OMt: I-OMt (a) and D-OMt (b).

or D-OMt, both masterbatches and crosslinked nanocomposites, contain OMt with stacked clay mineral layers or extensively delaminated OMt, respectively.

DSC analysis was performed on the masterbatches with I-OMt, finding a peak at about 46 °C, in line with what was found by analyzing pristine I-OMt. It is known that OMt with intercalated alkylammoniums give rise to endothermic transitions also in CPN (Carretero-Gonzalez et al., 2008; Ramorino et al., 2009).

TEM analysis was performed on a large number of masterbatches and crosslinked nanocomposites: even dispersion of both I-OMt

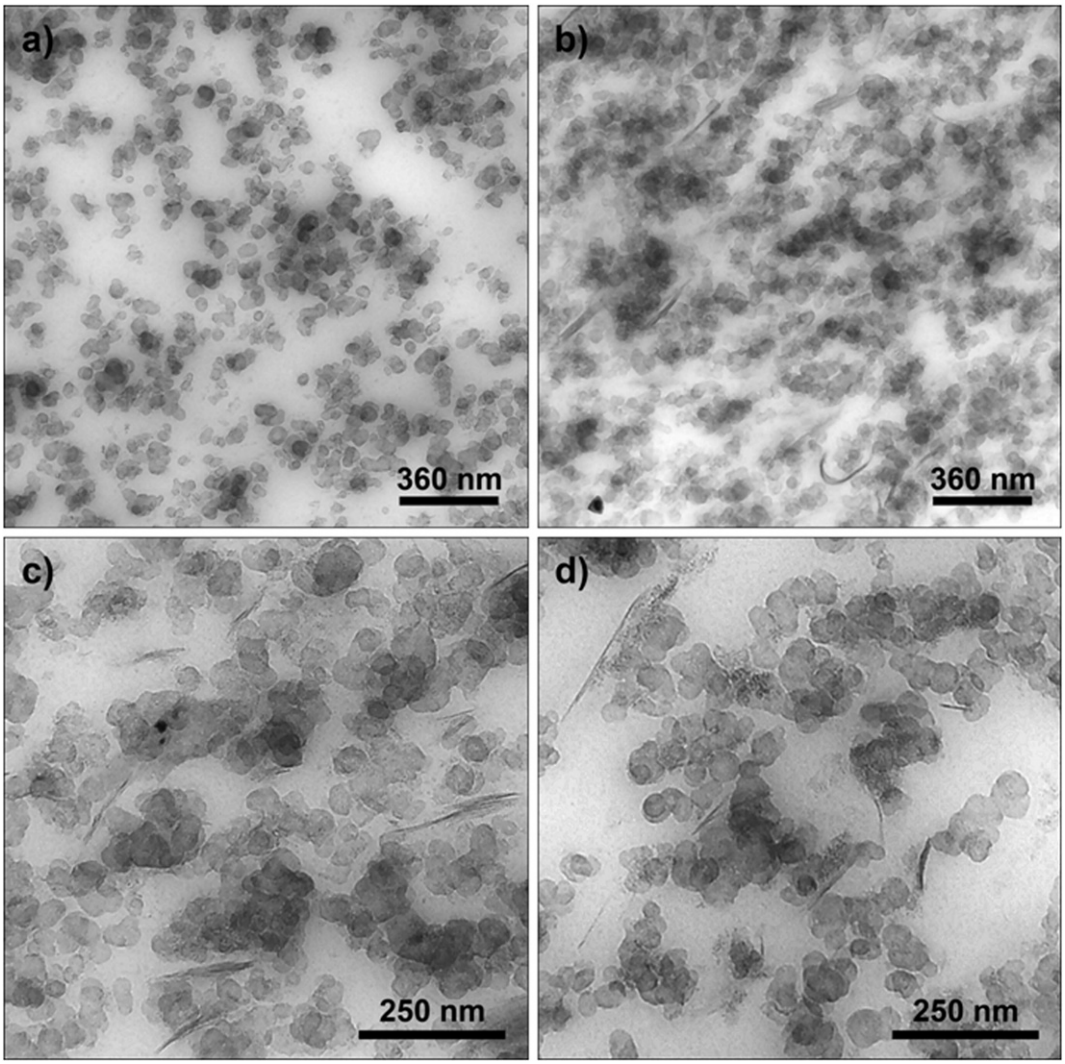

Fig. 4. TEM micrographs of PI-based nanocomposites, containing: CB (a), CB + I-OMt (b, c), and CB + D-OMt (d). All the masterbatches contain the silane.

and D-OMt was observed, especially in the nanocomposites. TEM micrographs of nanocomposites containing either I-OMt or D-OMt are reported in Fig. 4. CB dispersion was better in the presence of both OMt: the network formed by CB agglomerates is neither continuous nor homogenous in the absence of OMt (Fig. 4a). On the other hand, less and smaller CB agglomerates are present and the secondary network made by CB aggregates is fine and continuous in the presence of I-OMt (Fig. 4b). These findings are in line with what was recently reported (Galimberti et al., 2012, 2013b): OMt (prevailingly delaminated) was observed to promote a remarkable improvement of CB dispersion. The mutual distribution of CB and OMt can be better inspected in the micrographs taken at higher magnification.

In Fig. 4c, it appears that clay mineral stacks of I-OMt join together carbon black aggregates, thus forming a hybrid network. In the case of the nanocomposite with D-OMt (Fig. 4d), clay mineral layers appear to adhere to CB aggregates and do not form bridges between them.

3.3. Dynamic-mechanical properties of uncrosslinked composites

Dynamic-mechanical characterization was first performed on uncrosslinked masterbatches containing only PI, CB, OMt and the silane, to avoid the influence of further ingredients and of the crosslinking network. Dependence of shear storage modulus G′ and of loss storage modulus G″ on the shear strain, obtained from strain sweep tests performed at room temperature, is reported in Fig. 5a and b respectively. The standard deviation error bar is reported for the points of CB/D-OMt nanocomposite: there is no overlapping of the curve due to CB/D-OMt with any of the other curves, over the whole explored span of strain amplitudes.

It is evident that the replacement of part of CB (1/6 as mass ratio) with the same volume fraction of OMt led to substantial increase of the G′ modulus at low strain and that the CB/I-OMt system features the highest reinforcing effect. As a consequence, more pronounced reduction of the modulus with the increase of the strain amplitude is found with nanocomposites containing OMt, as the curves appear to converge at high strain amplitude, independently of the composition of the filler system. The reduction of the initial storage modulus with the strain amplitude (ΔG′ in this case) is a phenomenon known as Payne Effect (Payne, 1962; Payne and Whittaker, 1971), interpreted with agglomeration–de-agglomeration process of the filler network above the filler percolation threshold (Heinrich and Kluppel, 2002 and refs therein; Bohm et al., 2010) and/or with filler-matrix bonding and debonding mechanisms (Gauthier et al., 2004; Jancar and Douglas, 2010; Montes et al., 2003; Sternstein and Zhu, 2002). It was shown (Payne and Whittaker, 1971), that ΔG′ is linearly related with the maximum of the G″ loss modulus. In line with that, CPN containing OMt have higher G″ values, in particular when 2HT is intercalated between the Mt layers (CB/I-OMt sample, Fig. 5b). These findings lead to comment that, whatever is the mechanism at the origin of the Payne effect, the filler networking phenomenon is promoted by OMt and, in particu-lar, by I-OMt. This appears a counterintuitive result: in fact, D-OMt is expected to give a more pronounced filler networking phenomenon. TEM micrographs in Fig. 4c and d could help to explain these unexpect-ed experimental findings. They indicate that CB–OMt hybrid networks are formed more easily in the presence of I-OMt stacks. As a matter of fact, this could be justified considering that I-OMt has a higher effective volume fraction than D-OMt, as the intercalated alkylammoniums con-tribute to the I-OMt volume, whereas they essentially act, in D-OMt, as compatibilizers with the polymer matrix. Moreover, to interpret the higher modulus at low strain amplitude of the masterbatch with I-OMt, the crystallinity of I-OMt could be taken into account. In fact, as mentioned in the previous paragraph, an endothermic phenomenon, due to the loss of the rotator order of ammonium cation hydrocarbon tails (Cipolletti et al., 2014), was detected at about 45 °C.

The re-formation of the nanocomposites structure was then studied by first stretching the nanocomposite to large amplitude strain and then monitoring the increase, as a function of time, of the low amplitude nanocomposite modulus. Largely stretched filled polymer melts and elastomers are known to restore their original modulus in a time-dependent fashion, as their structure is re-established. The modulus recovery is considered to give information on the reformation of the ma-terial structure, altered by the stretch, and, in particular, on the mobility of the chains in proximity of the filler. In the present work, the objective was in particular to verify the persistency of the differences between nanocomposites based on either I-OMt or D-OMt. The time-dependent behavior of masterbatches containing OMt was thus studied by performing experiments of low strain amplitude ($\gamma = 0.003$) storage modulus recovery after the application of a large amplitude ($\gamma = 0.1$) dynamic strain. In Fig. 6a, the low amplitude storage modulus, measured after the application of the large strain perturbation, is plot-ted versus the logarithm of recovery time. It was shown that recovery data can be linearly interpolated for nanocomposites containing CB and I-OMt (Ramorino et al., 2007), as successfully done for other systems (Chazeau et al., 2000; Zhu and Sternstein, 2003). In Fig. 6b, it is reported the trend of the fractional recovery of low strain amplitude ($\gamma = 0.003$) shear modulus as a function of the log of recovery time. Indicating with G'_0 and with G'_∞ the values of the storage modulus measured at low ($\gamma = 0.003$), and represented as dashed line in Fig. 6a, and high ($\gamma = 0.1$) strain amplitude, respec-tively, the fractional recovery is expressed as: $[G'(t) - G'_\infty]/[G'_0 - G'_\infty] \times 100$.

The fractional recovery curves of Fig. 6b show very similar recovery kinetics. It appears that masterbatches recover between 40 and 50% of

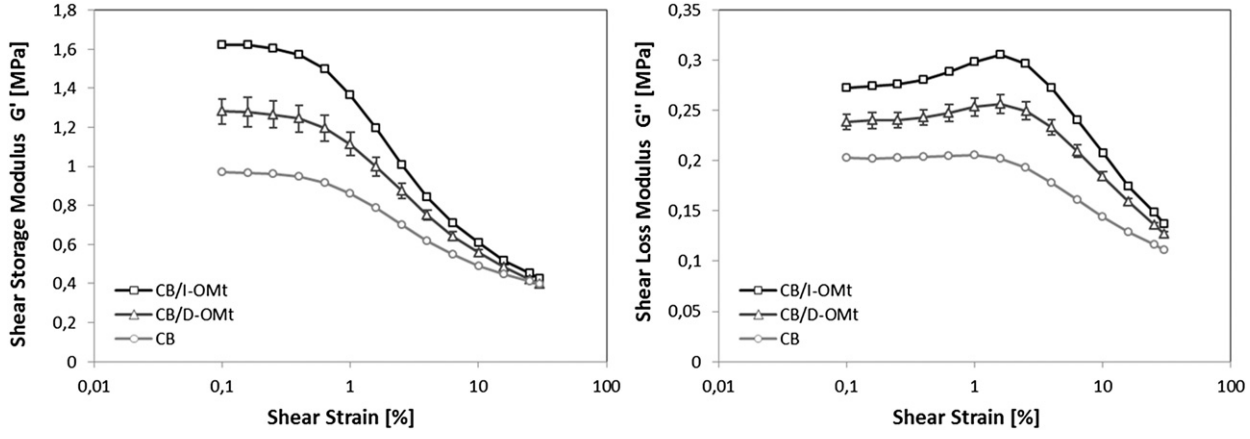

Fig. 5. Dynamic storage modulus G′ (a) and loss modulus (G″) in shear mode at 1 Hz plotted versus strain amplitude for PI based masterbatches, containing CB, OMt and silane.

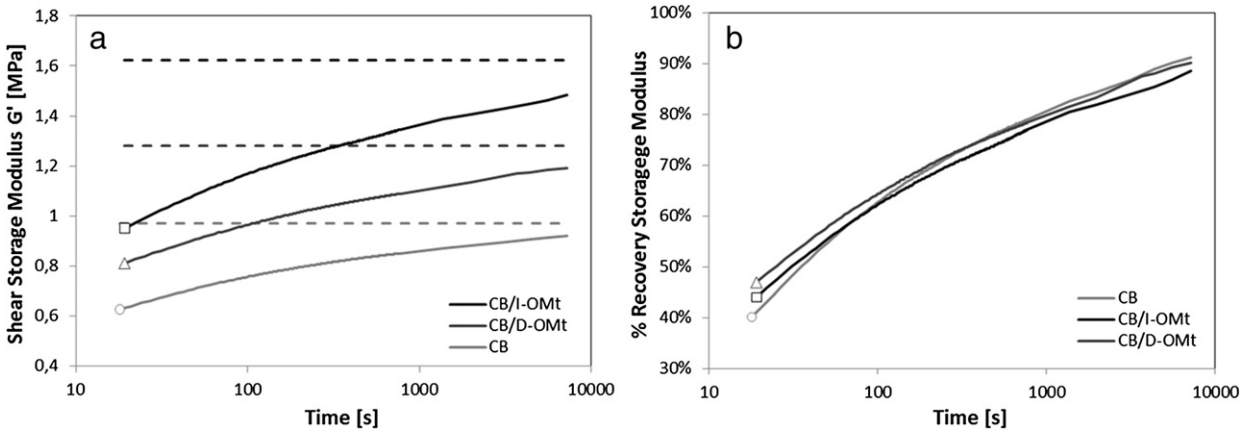

Fig. 6. Recovery (a) and fractional recovery (b) of low strain amplitude ($\gamma = 0.003$) shear modulus with time after the application of a high amplitude dynamic strain ($\gamma = 0.1$) for PI based masterbatches, containing CB(○), CB/D-OMt (Δ), CB/I-OMt (□) and silane.

the initial storage modulus 20 s after the removal of the large strain per-turbation. The sample without OMt shows a lower initial recovery and achieves, after few minutes, the same trend of the material with D-OMt and, at longer recovery times, the recovery rate of the system in-corporating I-OMt. It seems that the masterbatch with I-OMt reveals the need of longer time for recovering the initial value of the storage modulus. The chain mobility could be thus more affected by the hybrid network formed by CB and I-OMt. It is evident that the mechanisms of sorption/desorption of polymer chains on OC would deserve further investigations. However, the different structures of materials based on only CB, CB/I-OMt, and CB/D-OMt are reformed.

To further investigate the differences of polymer chain mobility in the presence of CB, CB/I-OMt, CB/D-OMt, the kinetics of relaxation of the small amplitude modulus was examined. In fact, in the literature, the enhancement of modulus due to the addition of a filler to polymer melt or elastomer has been attributed to large-scale conformational changes of polymer chains and to the reduction of their conformational entropy (Sternstein and Zhu, 2002). It was shown that the relaxation process of polymer chains was extended to longer times (Sternstein et al., 2010), also in presence of low filler concentrations.

Multifrequency dynamic mechanical analysis were carried out on masterbatches containing only PI, CB, OMt and the silane, obtaining a master-curve representation of G′ as a function of frequency, applying the procedure described in the experimental part. They are shown in Fig. 7.

It appears that the master curves of masterbatches with only CB as the filler and with CB/D-OMt hybrid filler system are almost overlapped, with a shorter and steeper plateau for the system incorporating only CB,

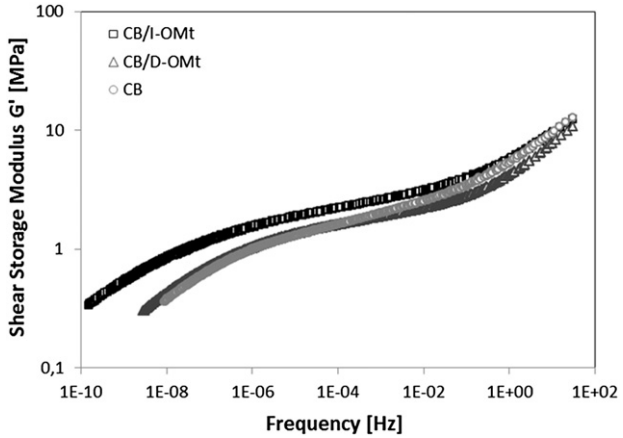

Fig. 7. Master curves for PI based masterbatches, containing CB, OMt and silane.

leading to higher modulus values on the high frequencies region. Clearly different is the master curve of the masterbatch containing I-OMt. The rubbery plateau has a lower slope and a major extension: the low fre-quency end of the master curve is expanded. The hybrid filler system CB/I-OMt appears to restrain the mobility of polymer chains, in line with the higher ability of such system to promote *the modulus enhance-ment, as consequence of a more effective filler networking via the immobilized polymer chains*.

Results discussed so far were obtained from masterbatches containing only CB, OMt and the silane. The effect of the other ingredients (listed in Table 1)onthefiller networking phenomenon was investigated by performing strain sweep measurements on uncrosslinked composites, observing the dependence of dynamic moduli on the shear strain. The G′ modulus as a function of the strain amplitude for uncrosslinked composites, containing either only CB or CB/I-OMt as filler systems, is reported in Fig. 8. I-OMt was selected as the OMt able to promote most pronounced filler networking phenomenon. Curves re-ferring to uncrosslinked masterbatches are reported for comparison. Masterbatches with I-OMt achieve higher values of G′ modulus at low strain, as already shown in Fig. 5a, whereas curves of the uncrosslinked composites are almost overlapped. The typical ingredients of an elastomeric composites appear thus to improve the dispersion of OMt in the polymer matrix, leading to the reduction of the filler networking. The analysis of a large number of TEM micrographs supported this

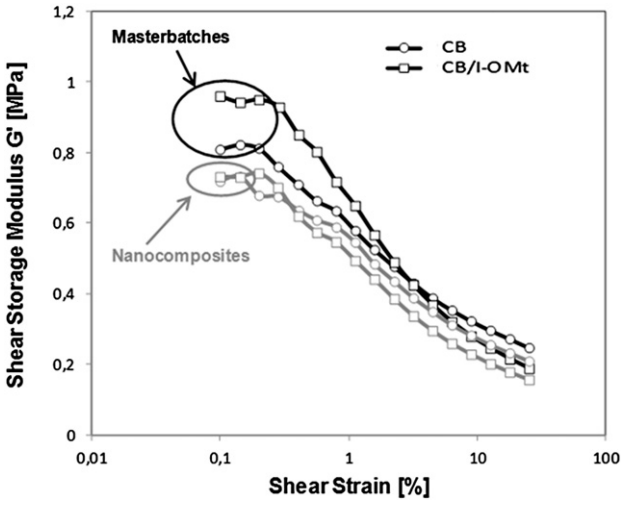

Fig. 8. Dynamic storage modulus G′ in shear mode at 1 Hz plotted versus strain amplitude for PI based masterbatches and uncrosslinked composites containing CB or CB/I-OMt.

comment: both I-OMt and D-OMt were observed to be more evenly dispersed in nanocomposites rather than in masterbatches.

3.4. Dynamic-mechanical properties of crosslinked composites

Dynamic-mechanical properties were investigated also on composites crosslinked with a typical sulfur based formulation (Coran, 2005). It is known that the compensating ammonium cations of OMt bring about noticeable acceleration of sulfur based crosslinking reaction (Avalos et al., 2008; Maiti et al., 2008; Sengupta et al., 2007; Verdejo et al., 2011). The tertiary amines formed from the ammonium cations and the increased mobility of sulfur accelerating anionic species are considered to be responsible of this phenomenon (Giannini et al., 2011). To prevent premature crosslinking and too fast kinetics, a combination of pre-vulcanization inhibitors, phthalic anhydride and *N*-cyclohexylthiophtalimide (Giannini et al., 2005) was used in this work. Composites were properly crosslinked, as shown by the values determined for the crosslinking parameters: ts1 and T90 were about 6 and 20 min, respectively, when CB was the only filler and about 3 and 18 min respectively, for the OMt based nanocomposites. Reversion reactions were not observed for any of the composites. Moreover, it is known that the interaction of the ammonium cations with thiolates leads to a reduction of the length of sulfur bridges between the polymer chains and thus to the increase of crosslinking network. A higher network density is known to lead to a higher modulus of the polymer composite (Donnet and Custodero, 2005).

Dependence of shear storage modulus G′ and loss storage modulus G″ on the shear strain, obtained from strain sweep tests performed at room temperature, are shown in Fig. 9a and 9b respectively. Standard deviation error bars are reported for the three curves: they reveal the reliability of the collected data. Curves of G′ vs strain for crosslinked composites with only CB and with CB/I-OMt are almost overlapped, whereas G′ values at low strain amplitudes are appreciably lower for the nanocomposite with CB/D-OMt. As the G′ values at high strain appear to be substantially the same for the three composites, the reduction of G′ with strain is larger for composites with CB and with CB/I-OMt. These findings seem to be not in line with what is shown in Fig. 5 where the Payne effect of the masterbatches (i.e., uncured compounds) appeared to follow the order: PI/CB/I-OMt > PI/CB/D-OMt > PI/CB. To ex-plain these apparently contradictory findings, one has to take into consideration that polar ingredients of elastomeric composites favor the dispersion of a polar filler such Mt (as shown in Fig. 8 and commented above). Curves of G″ vs strain are very similar for crosslinked composites with only CB and with CB/I-OMt whereas values of G″ for the nano-composites with CB/D-OMt are always lower (Fig. 9b). A more detailed inspection of curves in Fig. 9a and b reveals that OMt promotes the expansion of the plateau for G′ values at low strain amplitudes and the shift to higher strain amplitudes for the peak of G″ values. These findings are in line with what shown in Fig. 8 and indicate that the replacement of CB with an equal volume fraction of I-OMt has undetect-able effect on the filler networking phenomenon of nanocomposites with an even distribution of both CB and I-OMt. Moreover, it is con-firmed that the partial substitution of CB with D-OMt leads to a lower non linearity of the dynamic-mechanical properties of the nanocompos-ite. The different dynamic-mechanical behavior of nanocomposites containing CB and either I-OMt or D-OMt is thus reproduced, in masterbatches and in crosslinked materials.

The recovery of the storage modulus at low strain amplitude ($\gamma = 0.003$), after the application of a large amplitude ($\gamma = 0.1$) dynamic strain, was investigated also for the crosslinked composites.

For the three composites, about 65–70% of the modulus is recovered 20 s after the removal of the large strain perturbance. As expected, such recovery is larger than in the uncrosslinked masterbatches. The com-posite with CB shows a lower initial fractional recovery with, however, a higher recovery rate. The time needed to have a full recovery of the low amplitude modulus appears to be very similar for the three com-posites, that appear thus able to restore the original material structure. It is interesting to observe that, in spite of the fast recovery of the crosslinked systems, the full recovery of the small amplitude modulus still requires very long times. By comparing the curves of Fig. 10b with those of Fig. 6b, it is possible to see that the crosslinking mainly affects the short time recovery process, whereas, by extrapolating the curves at long times, both the crosslinked composites and the masterbatches seem to achieve complete recovery on the same time scale (between 10^4 and 10^5 s). This result is a possible consequence of the mechanisms taking place during recovery (Kalfus and Jancar, 2007). In particular, the restoring of the structure at the polymer–filler interface is probably the slowest one and affects in a similar manner the recovery times of all the systems, independently of polymer type and filler nature.

4. Conclusions

OMt are nowadays used in elastomeric materials, also for demanding dynamic-mechanical applications. In particular, large scale diffusion of OMt is achieved by using them in partial substitution of a traditional filler, such as CB. This work studied the correlation between the OMt organization and the dynamic-mechanical properties of polymer nanocomposites based on PI as the polymer matrix and CB as the main filler. Nanocomposites were prepared with two types of OMt: I-OMt, with ammonium cation intercalated between the clay mineral layers and D-OMt, obtained via ball milling of I-OMt. It is shown that OMt and CB form hybrid filler network and that I-OMt promote the filler networking phenomenon more easily than D-OMt. This is confirmed by a stronger reduction of the storage modulus with the strain amplitude

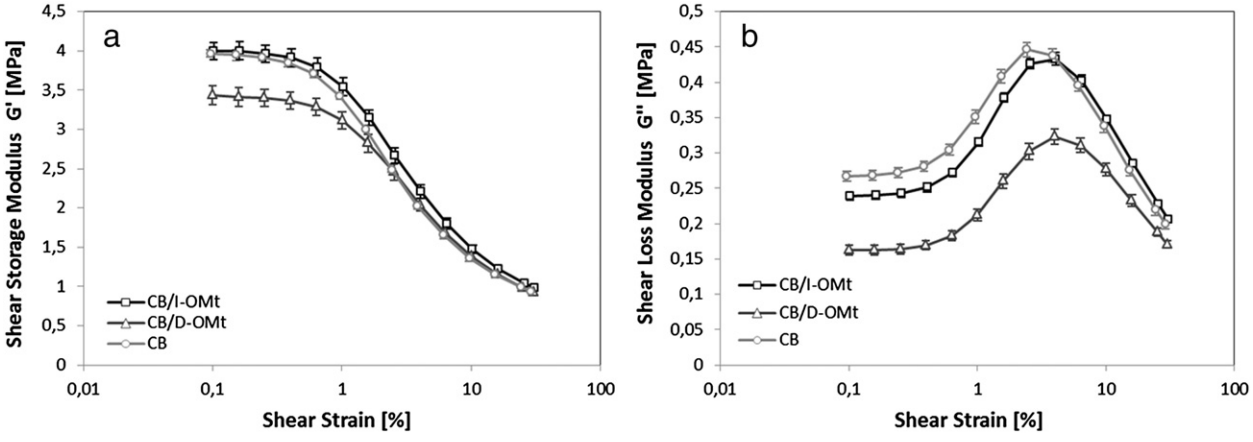

Fig. 9. Dynamic storage modulus G′ (a) and loss modulus (G″) in shear mode at 1 Hz plotted versus strain amplitude for crosslinked composites (see Table 1 for formulations).

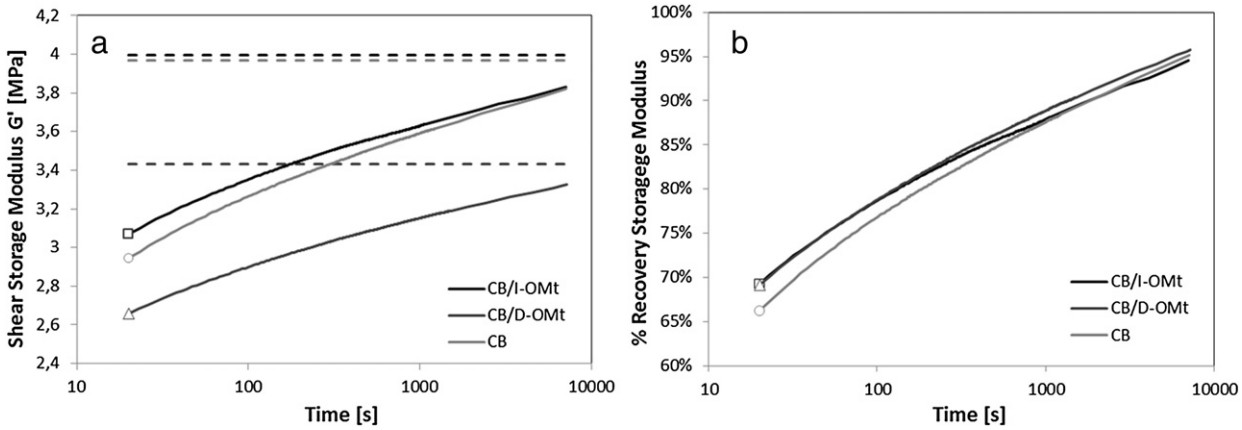

Fig. 10. Recovery (a) and fractional recovery (b) of low strain amplitude ($\gamma = 0.003$) shear modulus with time after the application of a high amplitude dynamic strain ($\gamma = 0.1$) for crosslinked composites (see Table 1 for formulations).

and by the expansion of the rubbery plateaus at low frequencies. The higher ability of I-OMt to form hybrid networks with CB was observed also in nanocomposites crosslinked with sulfur based systems. Results arising from the analyzed composition suggest that the partial replacement of CB with D-OMt gives a lower non linearity of the dynamic-mechanical properties of a crosslinked elastomeric compound having formulations close to the ones used for large scale applications.

The control of OMt organization and namely the extent of OMt delamination are presented as a key feature for reducing the dissipation of energy in dynamic-mechanical applications of polymer melts and elastomers containing a filler, such as CB, suitable to establish an intimate interaction with the organoclay.

References

Alexandre, M., Dubois, P., 2000. Polymer-layered silicate nanocomposites: preparation, properties and uses of a new class of materials. Mater. Sci. Eng. 28, 1–63.

Avalos, F., Ortiz, J.C., Zitzumbo, R., López-Manchado, M.A., Verdejo, R., Arroyo, M., 2008. Effect of montmorillonite intercalant structure on the cure parameters of natural rubber. Eur. Polym. J. 44, 3108–3115.

Bergaya, F.A., 2008. Layered clay minerals: basic research and innovative composite applications. Microporous Mesoporous Mater. 107, 141–148.

Bergaya, F., Lagaly, G., 2011. Intercalation processes of layered minerals. In: Brigatti, M.F.Mottana, A. (Eds.), Layered minerals structures and their application in advanced technologiesEuropean Mineralogical Union Notes in Mineralogy vol. 11. Mineralogi-cal Society, London, pp. 259–284 (Chapter 7).

Bergaya, F., Jaber, M., Lambert, J.F., 2011. Clays and clay minerals. In: Galimberti, M. (Ed.), Rubber Clay Nanocomposites: Science, Technology and Applications. Wiley, Chichester, pp. 3–44 (Chapter 1).

Bergaya, F., Jaber, M., Lambert, J.F., 2012. Clays and clay minerals as layered nanofillers for (bio)polymers. In: Averous, L., Pollet, E. (Eds.), Environmental Silicate Nano-biocomposites. Green Energy and Technology. Springer-Verlag, London, pp. 41–75 (Chapter 3).

Bhattacharya, M., Bhowmick, A.K., 2010. Synergy in carbon black-filled natural rubber nanocomposites. Part I: mechanical, dynamic mechanical properties, and morpholo-gy. J. Mater. Sci. 45, 6126–6138.

Bohm, G.A., Tomaszewski, W., Cole, W., Hogan, T., 2010. Furthering the understanding of the non linear response of filler reinforced elastomers. Polymer 51, 2057–2068.

Brochard-Wyart, F., De Gennes, P.-G., 2000. Viscosity at small scales in polymer melts. Eur. Phys. J. E 1, 93–97.

Carretero-Gonzalez, J., Retsos, H., Verdejo, R., Toki, S., Hsiao, B.S., Giannelis, E.P., López-Manchado, M.A., 2008. Effect of nanoclay on natural rubber microstructure. Macro-molecules 41, 6763–6772.

Cataldo, F., 2007. Preparation and properties of nanostructured rubber composites with montmorillonite. Macromol. Symp. 247, 67–77.

Chattopadhyay, P.K., Das, N.C., Chattopadhyay, S., 2011. Influence of interfacial roughness and the hybrid filler microstructures on the properties of ternary elastomeric composites. Compos. Part A 1049–1059.

Chazeau, L., Brown, J.D., Yanyo, L.C., Sternstein, S.S., 2000. Modulus recovery kinetics and other insights into the Payne effect for filled elastomers. Polym. Compos. 21, 202–220.

Chazhengina, S.Y., Kotelnikova, E.N., Filippova, I.V., Filatov, S.K., 2003. Phase transitions of *n*-alkanes as rotator crystals. J. Mol. Struct. 647, 243–257.

Chen, B., Evans, J.R.G., Greenwell, H.C., Boulet, P., Coveney, P.V., Bowden, A.A., Whiting, A., 2008. A critical appraisal of polymer–clay nanocomposites. Chem. Soc. Rev. 37, 568–594.

Christidis, G.E., Makri, P., Perdikatsis, V., 2004. Influence of grinding colour properties of on the structure and talc, bentonite and calcite white fillers. Clay Minerals 39, 163–175.

Cipolletti, V., Galimberti, M., Mauro, M., Guerra, G., 2014. Organoclays with hexagonal rotator order for the paraffinic chains of the compensating cation. Implications on the structure of clay polymer nanocomposites. Appl. Clay Sci. 87, 179–188.

Coran, A.Y., 2005. Vulcanization. In: Mark, J.E., Erman, B., Eirich, F.R. (Eds.), The Science and Technology of Rubber, Third ed. Elsevier Academic Press, Burlington (MA), pp. 321–366 (Chapter 7).

Das, A., Stoeckelhuber, K.W., Rooj, S., Wang, D.Y., Heinrich, G., 2010. Synergistic effects of expanded nanoclay and carbon black on natural rubber compounds. Kautsch. Gummi Kunst. 63, 296–302.

Dellisanti, F., Valdre, G., 2005. Study of structural properties of ion treated and mechanically deformed commercial bentonite. Appl. Clay Sci. 28, 233–244.

Donnet, J.B., Custodero, E., 2005. Reinforcement of elastomers by particulate fillers. In: Mark, J.E., Erman, B., Eirich, F.R. (Eds.), The Science and Technology of Rubber, Third ed. Elsevier Academic Press, Burlington (MA), pp. 367–400 (Chapter 8).

Feller, J.F., Bruzaud, S., Grohens, Y., 2004. Influence of clay nanofiller on electrical and rheological properties of conductive polymer composite. Mater. Lett. 58, 739–745.

Flores, F., Graebling, D., Allal, A., Guerret-Piecourt, C., 2007. Modelization of flow electrification in a polymer melt. J. Phys. D. Appl. Phys. 40, 2911–2919.

Fu, D., Liu, Y., Su, Y., Liu, G., Wang, D., 2011. Crystallization behavior of binary even–even-*n*-alkane mixtures in microcapsules: effect of composition and confined geometry on solid–solid phase separation. J. Phys. Chem. B 115, 4632–4938.

Galimberti, M. (Ed.), 2011. Rubber Clay Nanocomposites-science, Technology and Applications. Wiley and Sons, New York.

Galimberti, M., Lostritto, A., Spatola, A., Guerra, G., 2007. Clay delamination in hydrocarbon rubbers. Chem. Mater. 19, 2495–2499.

Galimberti, M., Senatore, S., Lostritto, A., Giannini, L., Conzatti, L., Costa, G., Guerra, G., 2009. Reinforcement of diene elastomers by organically modified layered silicates. e-Polymers 057, 1–16.

Galimberti, M., Coombs, M., Cipolletti, V., Riccio, P., Ricco, T., Pandini, S., Conzatti, L., 2012. Enhancement of mechanical reinforcement due to hybrid filler networking promoted by an organoclay in hydrocarbon-based nanocomposites. Appl. Clay Sci. 65–66, 57–66.

Galimberti, M., Coombs, M., Cipolletti, V., Giannini, L., Conzatti, L., 2013a. The origin of synergism between an organoclay and carbon black. Appl. Clay Sci. 83–84, 449–456.

Galimberti, M., Cipolletti, V., Mauro, M., Conzatti, L., 2013b. Nanocomposites of poly(1,4-*cis*-isoprene) with graphite oxide intercalation compounds. Macromol. Chem. Phys. 214, 1931–1939.

Galimberti, M., Cipolletti, V., Coombs, M., 2013c. Application of clay polymer nanocomposites. In: Bergaya, F., Lagaly, G. (Eds.), Handbook of clay science, 2nd Edi-tion Developments in Clay Science vol. 5. Elsevier, Amsterdam, pp. 539–586 (Chapter 4.4).

Galimberti, M., Coombs, M., Cipolletti, V., Riccò, T., Agnelli, S., Pandini, S., 2013d. The role of nanofillers in promoting hybrid filler networking and synergism with carbon black in a hydrocarbon rubber. Kautsch. Gummi Kunst. 66, 31–36.

Gates, W.P., 2004. Crystalline swelling of organo-modified clays in ethanol–water solutions. Appl. Clay Sci. 27, 1–12.

Gauthier, C., Reynaud, E., Vassoille, R., Ladouce-Stelandre, L., 2004. Analysis of the non-linear viscoelastic behaviour of silica filled styrene butadiene rubber. Polymer 45, 2761–2771.

Giannini, L., Fino, L., Galimberti, M., Citterio, A., 2005. International patent application WO07/062671 to Pirelli Tyre.

Giannini, L., Citterio, A., Galimberti, M., 2011. Chemistry of rubber/organoclay nanocomposites. In: Galimberti, M. (Ed.), Rubber Clay Nanocomposites — Science. Technology and Applications. Wiley and Sons, New York, pp. 127–146 (Chapter 5).

Gopi, J.A., Patel, S.K., Chandra, A.K., Tripathy, D.K., 2011. SBR–clay–carbon black hybrid nanocomposites for tire tread application. J. Polym. Res. 18, 1625–1634.

Heinrich, G., Kluppel, M., 2002. Recent advances in the theory of filler networking in elastomers. Adv. Polym. Sci. 160, 1–44.
Hrachova, J., Komadel, P., Fajnor, V.S., 2007. The effect of mechanical treatment on the structure of montmorillonite. J. Colloid Interface Sci. 61, 3361–3365.
Itoh, T., Ohta, N., Shichi, T., Yui, T., Takagi, K., 2003. The self-assembling properties of stearate ions in hydrotalcite clay composites. Langmuir 19, 9120–9126.
Jancar, J., Douglas, J.F., 2010. Current issues in research on structure–property relation ships in polymer nanocomposites. Polymer 51, 3321–3343.
Kalfus, J., Jancar, J., 2007. Viscoelastic response of nanocomposite poly(vinyl acetate)-hydroxyapatite with varying particle shape — dynamic strain softening and modulus recovery. Polym. Compos. 28, 743–747.
Konishi, Y., Cakmak, M., 2005. Structural hierarchy developed in injection molding of nylon 6/clay/carbon black nanocomposites. Polymer 46, 4811–4826.
Kvandea, I., Øyeb, G., Hammera, N., Rønninga, M., Raaenc, S., Holmena, A., Sjöblomb, J., Chen, D., 2008. Deposition of Au colloids on plasmachemically modified carbon nano-fibers. Carbon 46, 759–765.
Lagaly, G., Ogawa, M., Dekany, I., 2013. Clay mineral–organic interactions. In: Bergaya, F., Lagaly, G. (Eds.), Handbook of clay science, 2nd Edition Developments in Clay Science vol. 5. Elsevier, Amsterdam (Chapter 10.3).
LeBaron, P.C., Wang, Z., Pinnavaia, T.J., 1999. Polymer-layered silicate nanocomposites: an overview. Appl. Clay Sci. 15, 11–29.
Lin, J.J., Chu, C.C., Chiang, M.L., Tsai, W.C., 2006. First isolation of individual silicate platelets from clay exfoliation and their unique self-assembly into fibrous arrays. J. Phys. Chem. B 110, 18115–18120.
Maiti, M., Sadhu, S., Bhowmick, A.K., 2005. Effect of carbon black on properties of rubber nano-composites. J. Appl. Polym. Sci. 96, 443–451.
Maiti, M., Bhattacharya, M., Bhowmick, A.K., 2008. Elastomer nanocomposites. Rubber Chem. Technol. 81, 384–469.
Malas, A., Das, C.K., 2012. Carbon black–clay hybrid nanocomposites based upon EPDM elastomer. J. Mater. Sci. 47, 2016–2024.
Mauro, M., Maggio, M., Cipolletti, V., Galimberti, M., Longo, P., Guerra, G., 2013. Graphite oxide intercalation compounds with rotator hexagonal order in the intercalated layers. Carbon 61, 395–403.
Montes, H., Lequeux, F., Berriot, J., 2003. Influence of the glass transition temperature gradient on the nonlinear viscoelastic behavior in reinforced elastomers. Macromol-ecules 36, 8107–8118.
Osman, M.A., Ernst, M., Meier, B.H., Suter, U.W., 2002. Structure and molecular dynamics of alkane monolayers self-assembled on mica platelets. J. Phys. Chem. B 106, 653–662.
Paul, D.R., Robeson, L.M., 2008. Polymer nanotechnology: nanocomposites. Polymer 49, 3187–3204.
Payne, A.R., 1962. The dynamic properties of carbon black-loaded natural rubber vulcanizates. Part I J. Appl. Polym. Sci. 6, 57–63.
Payne, A.R., Whittaker, R.E., 1971. Low strain dynamic properties of filled rubbers. Rubber Chem. Technol. 44, 440–478.
Powder diffraction database 70–2151 International Centre for Diffraction Data. 1999 PCPDF win. Version 2.02.
Praveen, S., Chattopadhyay, P.K., Albert, P., Dalvi, V.G., Chakraborty, B.C., Chattopadhyay, S., 2009. Synergistic effect of carbon black and nanoclay fillers in styrene butadiene rub-ber matrix: development of dual structure. Compos. Part A 40, 309–316.
Ramadan, A.R., Esawi, A.M.K., Gawad, A.A., 2010. Effect of ball milling on the structure of Na+-montmorillonite and organo-montmorillonite (Cloisite 30B). Appl. Clay Sci. 47A, 196–202.
Ramorino, G., Bignotti, F., Conzatti, L., Riccò, T., 2007. Dynamic and viscoelastic behavior of natural rubber/layered silicate nanocomposites obtained by melt blending. Polym. Eng. Sci. 47, 1650–1657.
Ramorino, G., Bignotti, F., Pandini, S., Riccò, T., 2009. Mechanical reinforcement in natural rubber/organoclay nanocomposites. Compos. Sci. Technol. 69, 1206–1212.
Ray, S.S., Okamoto, M., 2003. Polymer/layered silicate nanocomposites: a review from preparation to processing. Progr. Polym. Sci. 28, 1539–1641.
Sabah, E., Mart, U., Cinar, M., Celik, M.S., 2007. Zeta potentials of sepiolite suspensions in concentrated monovalent electrolytes. Sep. Sci. Technol. 42, 2275–2288.
Sengupta, R., Chakraborty, S., Bandyopadhyay, S., Dasgupta, S., Mukhopadhyay, R., Auddy, K., Deuri, A.S., 2007. A short review on rubber/clay nanocomposites with emphasis on mechanical properties. Polym. Eng. Sci. 47, 1956–1974.
Sridhar, V., Shanmugharaj, A.M., Kim, J.K., Tripathy, D.K., 2009. Optimization of carbon black and nanoclay filler loading in chlorobutyl vulcanizates using response surface methodology. Polym. Compos. 30, 691–701.
Sternstein, S.S., Zhu, A.-J., 2002. Reinforcement mechanism of nanofilled polymer melts as elucidated by nonlinear viscoelastic behavior. Macromolecules 35, 7262–7273.
Sternstein, S.S., Amanuel, S., Shofner, M.L., 2010. Reinforcement mechanism in nanofilled polymer melts and elastomers. Rubber Chem. Technol. 83, 181–198.
Ungar, G., Masic, N., 1985. Order in the rotator phase of *n*-alkanes. J. Phys. Chem. 89, 1036–1042.
Verdejo, R., Hernandez, M., Bitinis, N., Kenny, J.M., Lopez-Manchado, M.A., 2011. Vulcani zation characteristics and curing kinetic of rubber/organoclay nanocomposites. In: Galimberti, M. (Ed.), Rubber Clay Nanocomposites — Science. Technology and Applications. Wiley and Sons, New York, pp. 275–304 (Chapter 9).
Xu, R., Wu, C., Xu, H., 2007. Particle size and zeta potential of carbon black in liquid media. Carbon 45, 2806–2809.
Zhu, A.-J., Sternstein, S.S., 2003. Nonlinear viscoelasticity of nanofilled polymers: interfaces, chain statistics and properties recovery kinetics. Compos. Sci. Technol. 63, 1113–1126.